Non-Markovian dynamics of a qubit coupled to an Ising spin bath

Hari Krovi,[1] Ognyan Oreshkov,[2] Mikhail Ryazanov,[3] and Daniel A. Lidar[1,2,3]
[1]*Department of Electrical Engineering, University of Southern California, Los Angeles, California 90089, USA*
[2]*Department of Physics, University of Southern California, Los Angeles 90089, USA*
[3]*Department of Chemistry, University of Southern California, Los Angeles, California 90089, USA*
(Received 13 July 2007; published 28 November 2007)

We study the analytically solvable Ising model of a single qubit system coupled to a spin bath. The purpose of this study is to analyze and elucidate the performance of Markovian and non-Markovian master equations describing the dynamics of the system qubit, in comparison to the exact solution. We find that the time-convolutionless master equation performs particularly well up to fourth order in the system-bath coupling constant, in comparison to the Nakajima-Zwanzig master equation. Markovian approaches fare poorly due to the infinite bath correlation time in this model. A recently proposed post-Markovian master equation performs comparably to the time-convolutionless master equation for a properly chosen memory kernel, and outperforms all the approximation methods considered here at long times. Our findings shed light on the applicability of master equations to the description of reduced system dynamics in the presence of spin baths.

DOI: 10.1103/PhysRevA.76.052117 PACS number(s): 03.65.Yz, 42.50.Lc

I. INTRODUCTION

A major conceptual as well as technical difficulty in the practical implementation of quantum information processing and quantum control schemes is the unavoidable interaction of quantum systems with their environment. This interaction can destroy quantum superpositions and lead to an irreversible loss of information, a process generally known as decoherence. Understanding the dynamics of open quantum systems is therefore of considerable importance. The Schrödinger equation, which describes the evolution of closed systems, is generally inapplicable to open systems, unless one includes the environment in the description. This is, however, generally difficult, due to the large number of environment degrees of freedom. An alternative is to develop a description for the evolution of only the subsystem of interest. A multitude of different approaches have been developed in this direction, exact as well as approximate [1,2]. Typically the exact approaches are of limited practical usefulness as they are either phenomenological or involve complicated integrodifferential equations. The various approximations lead to regions of validity that have some overlap. Such techniques have been studied for many different models, but their performance in general, is not fully understood.

In this work we consider an exactly solvable model of a single qubit (spin-1/2 particle) coupled to an environment of qubits. We are motivated by the physical importance of such spin bath models [3] in the description of decoherence in solid state quantum information processors, such as systems based on the nuclear spin of donors in semiconductors [4,5], or on the electron spin in quantum dots [6]. Rather than trying to accurately model decoherence due to the spin bath in such systems (as in, e.g., Refs. [7,8]), our goal in this work is to compare the performance of different master equations which have been proposed in the literature. Because the model we consider is exactly solvable, we are able to accurately assess the performance of the approximation techniques that we study. In particular, we study the Born-Markov and Born master equations, and the perturbation expansions of the Nakajima-Zwanzig (NZ) [9,10] and the time-convolutionless (TCL) master equations [11,12] up to fourth order in the coupling constant. We also study the post-Markovian (PM) master equation proposed in [13].

The dynamics of the system qubit in the model we study is highly non-Markovian and hence we do not expect the traditional Markovian master equations commonly used, e.g., in quantum optics [14] and nuclear magnetic resonance [15], to be accurate. This is typical of spin baths, and was noted, e.g., by Breuer *et al.* [16]. Several other papers deal with the effects of non-Markovian dynamics, some of which can be found in Refs. [17–25]. The work by Breuer *et al.* (as well as by other authors in a number of subsequent publications [26–31]) is conceptually close to ours in that in both cases an analytically solvable spin-bath model is considered and the analytical solution for the open system dynamics is compared to approximations. However, there are also important differences, namely, in Ref. [16] a so-called spin-star system was studied, where the system spin has equal couplings to all the bath spins, and these are of the *XY* exchange type. In contrast, in our model the system spin interacts via Ising couplings with the bath spins, and we allow for arbitrary coupling constants. As a result there are also important differences in the dynamics. For example, unlike the model in Ref. [16], for our model we find that the odd order terms in the perturbation expansions of Nakajima-Zwanzig and time-convolutionless master equations are nonvanishing. This reflects the fact that there is a coupling between the x and y components of the Bloch vector, which is absent in [16]. In view of the non-Markovian behavior of our model, we also discuss the relation between a representation of the analytical solution of our model in terms of completely positive maps, and the Markovian limit obtained via a coarse-graining method introduced in [32], and the performance of the post-Markovian master equation [13].

This paper is organized as follows. In Sec. II, we present the model, derive the exact solution, and discuss its behavior in the limit of small times and large number of bath spins, and in the cases of discontinuous spectral density co-domain and alternating sign of the system-bath coupling constants. In

Sec. III, we consider second order approximation methods such as the Born-Markov and Born master equations, and a coarse-graining approach to the Markovian semigroup master equation. Then we derive solutions to higher order corrections obtained from the Nakajima-Zwanzig and time-convolutionless projection techniques as well as derive the optimal approximation achievable through the post-Markovian master equation. In Sec. IV, we compare these solutions for various parameter values in the model and plot the results. Finally, in Sec. V, we present our conclusions.

II. EXACT DYNAMICS

A. Model

We consider a single spin-$\frac{1}{2}$ system (i.e., a qubit with a two-dimensional Hilbert space $\mathcal{H}_S$) interacting with a bath of N spin-$\frac{1}{2}$ particles (described by an N-fold tensor product of two-dimensional Hilbert spaces denoted $\mathcal{H}_B$). We model the interaction between the system qubit and the bath by the Ising Hamiltonian

$$H_I' = \alpha\sigma^z \otimes \sum_{n=1}^{N} g_n \sigma_n^z, \tag{1}$$

where g_n are dimensionless real-valued coupling constants in the interval $[-1,1]$, and $\alpha>0$ is a parameter having the dimension of frequency (we work in units in which $\hbar=1$), which describes the coupling strength and will be used below in conjunction with time (αt) for perturbation expansions. The system and bath Hamiltonians are

$$H_S = \frac{1}{2}\omega_0 \sigma^z, \tag{2}$$

and

$$H_B = \sum_{n=1}^{N} \frac{1}{2}\Omega_n \sigma_n^z. \tag{3}$$

For definiteness, we restrict the frequencies ω_0 and Ω_n to the interval $[-1,1]$, in inverse time units. Even though the units of time can be arbitrary, by doing so we do not lose generality, since we will be working in the interaction picture where only the frequencies Ω_n appear in relation to the state of the bath [Eq. (12)]. Since the ratios of these frequencies and the temperature of the bath occur in the equations, only their values relative to the temperature are of interest. Therefore, henceforth we will omit the units of frequency and temperature and will treat these quantities as dimensionless.

The interaction picture is defined as the transformation of any operator

$$A \mapsto A(t) = \exp(iH_0 t) A \exp(-iH_0 t), \tag{4}$$

where $H_0=H_S+H_B$. The interaction Hamiltonian H_I chosen here is invariant under this transformation since it commutes with H_0. [Note that in the next subsection, to simplify our calculations we redefine H_S and H_I' (whence H_I' becomes H_I), but this does not alter the present analysis.] All the quantities discussed in the rest of this paper are assumed to be in the interaction picture.

The dynamics can be described using the superoperator notation for the Liouville operator

$$\mathcal{L}\rho(t) \equiv -i[H_I', \rho(t)], \tag{5}$$

where $\rho(t)$ is the density matrix for the total system in the Hilbert space $\mathcal{H}_S \otimes \mathcal{H}_B$. The dynamics is governed by the von Neumann equation

$$\frac{d}{dt}\rho(t) = \alpha\mathcal{L}\rho(t), \tag{6}$$

and the formal solution of this equation can be written as follows:

$$\rho(t) = \exp(\alpha\mathcal{L}t)\rho(0). \tag{7}$$

The state of the system is given by the reduced density operator

$$\rho_S(t) = \mathrm{Tr}_B\{\rho(t)\}, \tag{8}$$

where Tr_B denotes a partial trace taken over the bath Hilbert space $\mathcal{H}_B$. This can also be written in terms of the Bloch sphere vector

$$\vec{v}(t) = \begin{pmatrix} v_x(t) \\ v_y(t) \\ v_z(t) \end{pmatrix} = \mathrm{Tr}\{\vec{\sigma}\rho_S(t)\}, \tag{9}$$

where $\vec{\sigma} \equiv (\sigma^x, \sigma^y, \sigma^z)$ is the vector of Pauli matrices. In the basis of σ^z eigenstates this is equivalent to

$$\rho_S(t) = \frac{1}{2}(I + \vec{v}\cdot\vec{\sigma}) = \frac{1}{2}\begin{pmatrix} 1+v_z(t) & v_x(t)-iv_y(t) \\ v_x(t)+iv_y(t) & 1-v_z(t) \end{pmatrix}. \tag{10}$$

We assume that the initial state is a product state, i.e.,

$$\rho(0) = \rho_S(0) \otimes \rho_B, \tag{11}$$

and that the bath is initially in the Gibbs thermal state at a temperature T,

$$\rho_B = \exp(-H_B/kT)/\mathrm{Tr}[\exp(-H_B/kT)], \tag{12}$$

where k is the Boltzmann constant. Since ρ_B commutes with the interaction Hamiltonian H_I, the bath state is stationary throughout the dynamics: $\rho_B(t)=\rho_B$. Finally, the bath spectral density function is defined as usual as

$$J(\Omega) = \sum_n |g_n|^2 \delta(\Omega - \Omega_n). \tag{13}$$

B. Exact solution for the system-spin dynamics

We first shift the system Hamiltonian in the following way:

$$H_S \mapsto H_S + \theta I,$$
$$\theta \equiv \mathrm{Tr}\left\{\sum_n g_n \sigma_n^z \rho_B\right\}. \tag{14}$$

As a consequence the interaction Hamiltonian is modified from Eq. (1) to

$$H_I' \mapsto H_I = \alpha\sigma^z \otimes B, \tag{15}$$

where

$$B \equiv \sum_n g_n\sigma_n^z - \theta I_B. \tag{16}$$

This shift is performed because now $\mathrm{Tr}_B[H_I,\rho(0)]=0$, or equivalently

$$\mathrm{Tr}_B\{B\rho_B\} = 0. \tag{17}$$

This property will simplify our calculations later when we consider approximation techniques in Sec. III. Now, we derive the exact solution for the reduced density operator ρ_S corresponding to the system. We do this in two different ways. The Kraus operator sum representation is a standard description of the dynamics of a system initially decoupled from its environment and it will also be helpful in studying the coarse-graining approach to the quantum semigroup master equation. The second method is computationally more effective and is helpful in obtaining analytical expressions for $N \gg 1$.

1. Exact solution in the Kraus representation

In the Kraus representation the system state at any given time can be written as

$$\rho_S(t) = \sum_{i,j} K_{ij}\rho_S(0)K_{ij}^\dagger, \tag{18}$$

where the Kraus operators satisfy $\Sigma_{ij}K_{ij}^\dagger K_{ij}=I_S$ [33]. These operators can be expressed easily in the eigenbasis of the initial state of the bath density operator as

$$K_{ij} = \sqrt{\lambda_i}\langle j|\exp(-iH_I t)|i\rangle, \tag{19}$$

where the bath density operator at the initial time is $\rho_B(0)=\Sigma_i\lambda_i|i\rangle\langle i|$. For the Gibbs thermal state chosen here, the eigenbasis is the N-fold tensor product of the σ^z basis. In this basis

$$\rho_B = \sum_l \frac{\exp(-\beta E_l)}{Z}|l\rangle\langle l|, \tag{20}$$

where $\beta=1/kT$. Here

$$E_l = \sum_{n=1}^N \frac{1}{2}\hbar\Omega_n(-1)^{l_n}, \tag{21}$$

is the energy of each eigenstate $|l\rangle$, where $l=l_1l_2,\ldots,l_n$ is the binary expansion of the integer l, and the partition function is $Z=\Sigma_l\exp(-\beta E_l)$. Therefore, the Kraus operators become

$$K_{ij} = \sqrt{\lambda_i}\exp(-it\alpha\tilde{E}_i\sigma^z)\delta_{ij}, \tag{22}$$

where

$$\tilde{E}_i = \langle i|B|i\rangle = \sum_{n=1}^N g_n(-1)^{i_n} - \mathrm{Tr}\left\{\sum_n g_n\sigma_n^z\rho_B\right\}, \tag{23}$$

and $\lambda_i=\exp(-\beta E_i)/Z$. Substituting this expression for K_{ij} into Eq. (18) and writing the system state in the Bloch vector form given in Eq. (10), we obtain

$$\begin{aligned} v_x(t) &= v_x(0)C(t) - v_y(0)S(t), \\ v_y(t) &= v_x(0)S(t) + v_y(0)C(t), \\ v_z(t) &= v_z(0), \end{aligned} \tag{24}$$

where

$$\begin{aligned} C(t) &= \sum_i \lambda_i \cos 2\alpha\tilde{E}_i t, \\ S(t) &= \sum_i \lambda_i \sin 2\alpha\tilde{E}_i t. \end{aligned} \tag{25}$$

Equations (24) are the exact solution to the system dynamics of the above spin-bath model. We see that the evolution of the Bloch vector is a linear combination of rotations around the z axis. This evolution reflects the symmetry of the interaction Hamiltonian, which is diagonal in the z basis. By inverting Eqs. (24) for $v_x(0)$ or $v_y(0)$, we see that the Kraus map is irreversible when $C(t)^2+S(t)^2=0$. This will become important below, when we discuss the validity of the time-convolutionless approximation.

2. Alternative exact solution

Another way to derive the exact solution which is computationally more useful is the following. Since all σ_n^z commute, the initial bath density matrix factors and can be written as

$$\rho_B = \bigotimes_{n=1}^N \frac{\exp\left(-\frac{\Omega_n}{2kT}\sigma_n^z\right)}{\mathrm{Tr}\left[\exp\left(-\frac{\Omega_n}{2kT}\sigma_n^z\right)\right]} = \bigotimes_{n=1}^N \frac{1}{2}(I+\beta_n\sigma_n^z) \equiv \prod_{n=1}^N \rho_n, \tag{26}$$

where

$$\beta_n = \tanh\left(-\frac{\Omega_n}{2kT}\right), \tag{27}$$

and $-1\leq\beta_n\leq 1$. Using this, we obtain an expression for θ defined in Eq. (14),

$$\begin{aligned} \theta &= \mathrm{Tr}\left\{\sum_{n=1}^N g_n\sigma_n^z \bigotimes_{m=1}^N \frac{1}{2}(I+\beta_m\sigma_m^z)\right\} \\ &= \sum_{n=1}^N g_n\,\mathrm{Tr}\left\{\frac{1}{2}(\sigma_n^z+\beta_n I)\right\}\prod_{m\neq n}\mathrm{Tr}\left\{\frac{1}{2}(I+\beta_m\sigma_m^z)\right\} \\ &= \sum_{n=1}^N g_n\beta_n. \end{aligned} \tag{28}$$

The evolution of the system density matrix in the interaction picture is

$$\rho_S(t) = \mathrm{Tr}_B\{e^{-iH_I t}\rho(0)e^{iH_I t}\}. \tag{29}$$

In terms of the system density matrix elements in the computational basis $\{|0\rangle,|1\rangle\}$ (which is an eigenbasis of σ^z in $H_I=\alpha\sigma^z\otimes B$), we have

$$\langle j|\rho_S(t)|k\rangle = \langle j|\mathrm{Tr}_B\{e^{-iH_I t}\rho_S(0)\bigotimes_{m=1}^{N}\rho_m e^{iH_I t}\}|k\rangle$$

$$= \mathrm{Tr}_B\{e^{-i\alpha\langle j|\sigma^z|j\rangle Bt}\langle j|\rho_S(0)|k\rangle\bigotimes_{m=1}^{N}\rho_m e^{+i\alpha\langle k|\sigma^z|k\rangle Bt}\}.$$

Let us substitute $\langle j|\sigma^z|j\rangle=(-1)^j$ and rewrite

$$e^{-i\alpha\langle j|\sigma^z|j\rangle Bt} = e^{-i\alpha(-1)^j(\Sigma_{l=1}^{N}g_l\sigma_l^z-\theta I)t} = \bigotimes_{l=1}^{N} e^{-i(-1)^j\alpha[g_l\sigma_l^z-(\theta/N)I]t}.$$

Since all the matrices are diagonal, they commute and we can collect the terms by qubits as follows:

$$\langle j|\rho_S(t)|k\rangle = \langle j|\rho_S(0)|k\rangle\mathrm{Tr}\{\bigotimes_{m=1}^{N} e^{-i[(-1)^j-(-1)^k]\alpha[g_l\sigma_l^z-(\theta/N)I]t}\rho_n\}.$$

Let us denote $(-1)^j-(-1)^k=2\epsilon_{jk}$. The trace can be easily computed to be

$$\prod_{n=1}^{N}\mathrm{Tr}\left\{e^{-i2\epsilon_{jk}\alpha[g_n\sigma_n^z-(\theta/N)I]t}\frac{1}{2}(I+\beta_n\sigma_n^z)\right\}$$

$$= \prod_{n=1}^{N} e^{i2\epsilon_{jk}\alpha(\theta/N)t}[\cos(2\epsilon_{jk}\alpha g_n t) - i\beta_n\sin(2\epsilon_{jk}\alpha g_n t)].$$

Thus the final expression for the system density matrix elements is

$$\langle j|\rho_S(t)|k\rangle = \langle j|\rho_S(0)|k\rangle e^{i2\epsilon_{jk}\alpha\theta t}\prod_{n=1}^{N}[\cos(2\epsilon_{jk}\alpha g_n t) - i\beta_n\sin(2\epsilon_{jk}\alpha g_n t)].$$

Notice that $\epsilon_{00}=\epsilon_{11}=0$, hence the diagonal matrix elements do not depend on time as before.

$$\langle 0|\rho_S(t)|0\rangle = \langle 0|\rho_S(0)|0\rangle,$$

$$\langle 1|\rho_S(t)|1\rangle = \langle 1|\rho_S(0)|1\rangle.$$

For the off-diagonal matrix elements $\epsilon_{01}=1$, $\epsilon_{10}=-1$, and the evolution is described by

$$\langle 0|\rho_S(t)|1\rangle = \langle 0|\rho_S(0)|1\rangle f(t),$$

$$\langle 1|\rho_S(t)|0\rangle = \langle 1|\rho_S(0)|0\rangle f^*(t), \tag{30}$$

where

$$f(t) = e^{i2\alpha\theta t}\prod_{n=1}^{N}[\cos(2\alpha g_n t) - i\beta_n\sin(2\alpha g_n t)]. \tag{31}$$

In terms of the Bloch vector components, this can be written in the form of Eq. (24), where

$$C(t) = [f(t)+f^*(t)]/2,$$

$$S(t) = [f(t)-f^*(t)]/2i. \tag{32}$$

C. Limiting cases

1. Short times

Consider the evolution for short times where $\alpha t \ll 1$. Then

$$\left|\prod_{n=1}^{N}[\cos(2\alpha g_n t) \pm i\beta_n\sin(2\alpha g_n t)]\right|$$

$$= \prod_{n=1}^{N}\sqrt{1-(1-\beta_n^2)\sin^2(2\alpha g_n t)}$$

$$\approx \prod_{n=1}^{N}[1-2(1-\beta_n^2)(\alpha g_n t)^2]$$

$$\approx 1-2\left[\alpha^2\sum_{n=1}^{N} g_n^2(1-\beta_n^2)\right]t^2$$

$$\approx \exp[-2(\alpha t)^2 Q_2], \tag{33}$$

where (see Appendix A)

$$Q_2 \equiv \mathrm{Tr}\{B^2\rho_B\} = \sum_{n=1}^{N} g_n^2(1-\beta_n^2) = \int_{-\infty}^{\infty}\frac{2J(\Omega)}{1+\cosh\left(\frac{\Omega}{kT}\right)}d\Omega. \tag{34}$$

Note that the above approximation is valid under any of the following conditions: very short times ($\alpha t \ll 1\sqrt{Q_2}$), low temperatures ($Q_2 \ll 1$), or a large number of qubits and not too low temperatures $\sqrt{Q_2} \gg |g_n|, \forall n$ (see also below). The total phase of $f(t)$ in Eq. (31) is

$$\phi \approx 2\theta\alpha t + \sum_{n=1}^{N}(-\beta_n 2\alpha g_n t) = 2\theta\alpha t - 2\alpha\left(\sum_{n=1}^{N} g_n\beta_n\right)t = 0, \tag{35}$$

where we have used Eq. (28). Thus, the off-diagonal elements of the system density matrix become

$$\rho_S^{01}(t) \approx \rho_S^{01}(0)e^{-2(\alpha t)^2 Q_2},$$

$$\rho_S^{10}(t) \approx \rho_S^{10}(0)e^{-2(\alpha t)^2 Q_2}. \tag{36}$$

Finally, the dynamics of the Bloch vector components are

$$v_{x,y}(t) \approx v_{x,y}(0)e^{-2(\alpha t)^2 Q_2},$$

$$v_z(t) = v_z(t). \tag{37}$$

This represents the well known behavior [34] of the evolution of an open quantum system in the Zeno regime. In this regime coherence does not decay exponentially but is initially flat, as is the case here due to the vanishing time derivative of $\rho_S^{01}(t)$ at $t=0$. As we will see in Sec. III, the dynamics in the Born approximation (which is also the second order time-convolutionless approximation) exactly matches the last result.

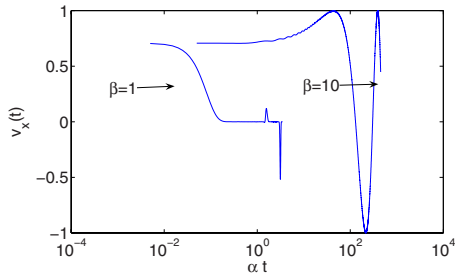

FIG. 1. (Color online) Comparison of the exact solution at $\beta=1$ and $\beta=10$ for $N=100$.

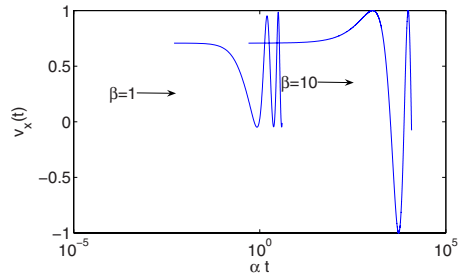

FIG. 2. (Color online) Comparison of the exact solution at $\beta=1$ and $\beta=10$ for $N=4$.

2. Large N

When $N \gg 1$ and the values of g_n are random, then the different terms in the product of Eq. (31) are smaller than 1 most of the time and have recurrences at different times. Therefore, we expect the function $f(t)$ to be close to zero in magnitude for most of the time and full recurrences, if they exist, to be extremely rare. When g_n are equal and so are Ω_n, then partial recurrences occur periodically, independently of N. Full recurrences occur with a period which grows at least as fast as N. This can be argued from Eqs. (24) by imposing the condition that the arguments of all the cosines and sines are simultaneously equal to an integer multiple of 2π. When $J(\Omega)$ has a narrow high peak, e.g., one g_n is much larger than the others, then the corresponding terms in the products in Eq. (31) oscillate faster than the rate at which the whole product decays. This is effectively a modulation of the decay.

3. Discontinuous spectral density co-domain

As can be seen from Eq. (31), the coupling constants g_n determine the oscillation periods of the product terms, while the temperature factors β_n determine their modulation depths. If the codomain of spectral density is not continuous, i.e., it can be split into nonoverlapping intervals G_j, $j=1,\ldots,J$, then Eq. (31) can be represented in the following form:

$$f(t) = e^{i2\alpha\theta t} P_1(t) P_2(t) \cdots P_J(t), \tag{38}$$

where

$$P_j(t) = \prod_{g_n \in G_j} [\cos(2\alpha g_n t) - i\beta_n \sin(2\alpha g_n t)]. \tag{39}$$

In this case, if G_j are separated by large enough gaps, the evolution rates of different $P_j(t)$ can be significantly different. This is particularly noticeable if one $P_j(t)$ undergoes partial recurrences while another $P_{j'}(t)$ slowly decays.

For example, one can envision a situation with two intervals such that one term shows frequent partial recurrences that slowly decay with time, while the other term decays faster, but at times larger than the recurrence time. The overall evolution then consists of a small number of fast partial recurrences. In an extreme case, when one g_n is much larger than the others, this results in an infinite harmonic modulation of the decay with depth dependent on β_n, i.e., on temperature.

4. Alternating signs

If the bath has the property that every bath qubit m has a pair $-m$ with the same frequency $\Omega_{-m}=\Omega_m$, but opposite coupling constant $g_{-m}=-g_m$, the exact solution can be simplified. First, $\beta_{-m}=\beta_m$, and $\theta=0$. Next, Eq. (31) becomes

$$\begin{aligned} f(t) &= \prod_{m=1}^{N/2} [\cos(2\alpha g_m t) - i\beta_m \sin(2\alpha g_m t)][\cos(2\alpha g_{-m} t) \\ &\quad - i\beta_{-m} \sin(2\alpha g_{-m} t)] \\ &= \prod_{m=1}^{N/2} [\cos^2(2\alpha g_m t) + \beta_m^2 \sin^2(2\alpha g_m t)]. \end{aligned} \tag{40}$$

This function is real, thus Eq. (32) becomes $C(t)=f(t)$, $S(t)=0$, so that $v_x(t)=v_x(0)f(t)$ and $v_y(t)=v_y(0)f(t)$. The exact solution is then symmetric under the interchange $v_x \leftrightarrow v_y$, a property shared by all the second order approximate solutions considered below, as well as the post-Markovian master equation. The limiting case Eq. (33) remains unchanged, and since Q_2 depends on g_n^2, but not g_n, it and all second order approximations also remain unchanged. In the special case $|g_m|=g$, the exact solution exhibits full recurrences with period $T=\pi/\alpha g$.

III. APPROXIMATION METHODS

In this section we discuss the performance of different approximation methods developed in the open quantum systems literature [1,2]. The corresponding master equations for the system density matrix can be derived explicitly and since the model considered here is exactly solvable, we can compare the approximations to the exact dynamics. We use the Bloch vector representation and since the z component has no dynamics, a fact which is reflected in all the master equations, we omit it from our comparisons.

A. Born and Born-Markov approximations

Both the Born and Born-Markov approximations are second order in the coupling strength α.

1. Born approximation

The Born approximation is equivalent to a truncation of the Nakajima-Zwanzig projection operator method at the second order, which is discussed in detail in Sec. III B. The

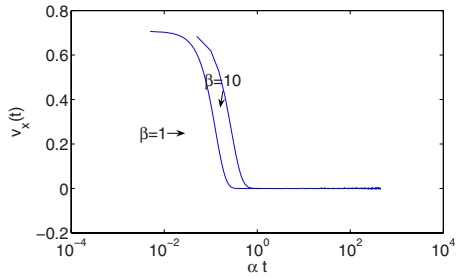

FIG. 3. (Color online) Comparison of the exact solution at $\beta=1$ and $\beta=10$ for $N=100$ for randomly generated g_n and Ω_n.

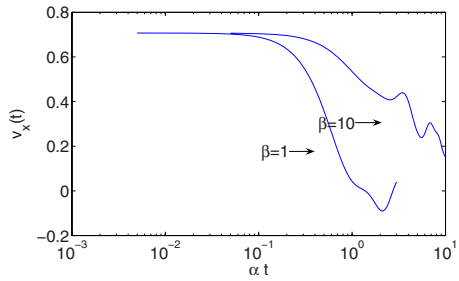

FIG. 4. (Color online) Comparison of the exact solution at $\beta=1$ and $\beta=10$ for $N=4$ for randomly generated g_n and Ω_n.

Born approximation is given by the following integrodifferential master equation:

$$\dot{\rho}_S(t) = -\int_0^t \mathrm{Tr}_B\{[H_I(t),[H_I(s),\rho_S(s)\otimes\rho_B]]\}ds. \quad (41)$$

Since in our case the interaction Hamiltonian is time independent, the integral becomes easy to solve. We obtain

$$\dot{\rho}_S(t) = -2\alpha^2 Q_2 \int_0^t [\rho_S(s) - \sigma^z\rho_S(s)\sigma^z]ds, \quad (42)$$

where Q_2 is the second order bath correlation function in Eq. (34). Writing $\rho_S(t)$ in terms of Bloch vectors as $(I+\vec{v}\cdot\vec{\sigma})/2$ [Eq. (10)], we obtain the following integrodifferential equations:

$$\dot{v}_{x,y}(t) = -4\alpha^2 Q_2 \int_0^t v_{x,y}(s)ds. \quad (43)$$

These equations can be solved by taking the Laplace transform of the variables. The equations become

$$sV_{x,y}(s) - v_{x,y}(0) = -4\alpha^2 Q_2 \frac{V_{x,y}(s)}{s}, \quad (44)$$

where $V_{x,y}(s)$ is the Laplace transform of $v_{x,y}(t)$. This gives

$$V_{x,y}(s) = \frac{v_{x,y}(0)s}{s^2 + 4Q_2\alpha^2}, \quad (45)$$

which can be readily solved by taking the inverse Laplace transform. Doing so, we obtain the solution of the Born master equation for our model as follows:

$$v_{x,y}(t) = v_{x,y}(0)\cos(2\alpha\sqrt{Q_2}t). \quad (46)$$

Note that this solution is symmetric under the interchange $v_x \leftrightarrow v_y$, but the exact dynamics in Eq. (24) does not have this symmetry. The exact dynamics respects the symmetry: $v_x \to v_y$ and $v_y \to -v_x$, which is a symmetry of the Hamiltonian. This means that higher order corrections are required to break the symmetry $v_x \leftrightarrow v_y$ in order to approximate the exact solution more closely.

One often makes the substitution $v_{x,y}(t)$ for $v_{x,y}(s)$ in Eq. (43) since the integrodifferential equation obtained in other models may not be as easily solvable. This approximation, which is valid for short times, yields

$$\dot{v}_{x,y}(t) = -4\alpha^2 Q_2 t v_{x,y}(t), \quad (47)$$

which gives

$$v_{x,y}(t) = v_{x,y}(0)\exp(-2Q_2\alpha^2 t^2), \quad (48)$$

i.e., we recover Eq. (37). This is the same solution obtained in the second-order approximation using the time-convolutionless (TCL) projection method discussed in Sec. III B.

2. Born-Markov approximation

In order to obtain the Born-Markov approximation, we use the following quantities [2, Ch. 3]:

$$R(\omega) = \sum_{E_2-E_1=\omega} P_{E_1}\sigma^z P_{E_2},$$

$$\Gamma(\omega) = \alpha^2 \int_0^\infty e^{i\omega s} Q_2 ds, \quad (49)$$

$$H_L = \sum_\omega T(\omega)R(\omega)^\dagger R(\omega),$$

where $T(\omega)=[\Gamma(\omega)-\Gamma(\omega)^*]/2i$, E_i is an eigenvalue of the system Hamiltonian H_S, and P_{E_i} is the projector onto the eigenspace corresponding to this eigenvalue. In our case H_S is diagonal in the eigenbasis of σ^z, and only $\omega=0$ is relevant. This leads to $R(0)=\sigma^z$ and $\Gamma(0)=\alpha^2\int_0^\infty Q_2 dt$. Since $\Gamma(0)$ is real, we have $T(0)=0$. Hence the Lamb shift Hamiltonian $H_L=0$, and the Lindblad form of the Born-Markov approximation is

$$\dot{\rho}_S(t) = \gamma(\sigma^z\rho_S\sigma^z - \rho_S), \quad (50)$$

where $\gamma=\Gamma(0)+\Gamma(0)^*=2\alpha^2\int_0^\infty Q_2 dt$. But note that $Q_2=\mathrm{Tr}_B\{B^2\rho_B\}$ does not depend on time. This means that Γ and hence γ are both infinite. Thus the Born-Markov approximation is not valid for this model and the main reason for this is the time independence of the bath correlation functions. The dynamics is inherently non-Markovian.

A different approach to the derivation of a Markovian semigroup master equation was proposed in [32]. In this approach, a Lindblad equation is derived from the Kraus operator-sum representation by a coarse-graining procedure defined in terms of a phenomenological coarse-graining time scale τ. The general form of the equation is

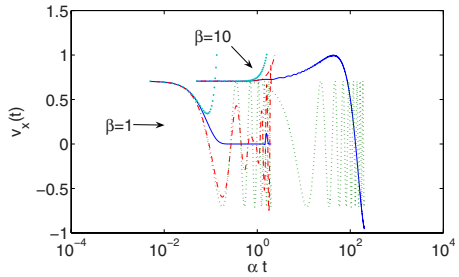

FIG. 5. (Color online) Comparison of the exact solution, NZ2, NZ3, and NZ4 at $\beta=1$ and $\beta=10$ for $N=100$. The exact solution is the solid (blue) line, NZ2 is the dashed (green) line, NZ3 is the dot-dashed (red) line, and NZ4 is the dotted (cyan) line.

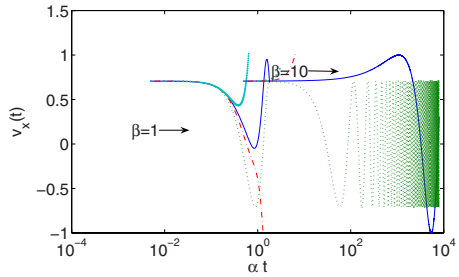

FIG. 6. (Color online) Comparison of the exact solution, NZ2, NZ3, and NZ4 at $\beta=1$ and $\beta=10$ for $N=4$. The exact solution is the solid (blue) line, NZ2 is the dashed (green) line, NZ3 is the dot-dashed (red) line, and NZ4 is the dotted (cyan) line.

$$\frac{\partial\rho(t)}{\partial t} = -i[\langle \dot{Q}\rangle_\tau, \rho(t)] + \frac{1}{2}\sum_{\alpha,\beta=1}^{M} \langle \dot{\chi}_{\alpha,\beta}\rangle_\tau ([A_\alpha, \rho(t)A_\beta^\dagger] + [A_\alpha \rho(t), A_\beta^\dagger]),$$

where the operators $A_0=I$ and A_α, $\alpha=1,\ldots,M$ form an arbitrary fixed operator basis in which the Kraus operators (18) can be expanded as

$$K_i = \sum_{\alpha=0}^{M} b_{i\alpha} A_\alpha. \tag{51}$$

The quantities $\chi_{\alpha,\beta}(t)$ and $Q(t)$ are defined through

$$\chi_{\alpha,\beta}(t) = \sum_i b_{i\alpha}(t) b_{i\beta}^*(t), \tag{52}$$

$$Q(t) = \frac{i}{2}\sum_{\alpha=1}^{M} [\chi_{\alpha 0}(t) K_\alpha - \chi_{0\alpha}(t) K_\alpha^\dagger], \tag{53}$$

and

$$\langle X\rangle_\tau = \frac{1}{\tau}\int_0^\tau X(s)ds. \tag{54}$$

For our problem we find

$$\frac{\partial\rho(t)}{\partial t} = -i\tilde{\omega}[\sigma_Z, \rho(t)] + \tilde{\gamma}[\sigma_Z \rho(t)\sigma_Z - \rho(t)], \tag{55}$$

where

$$\tilde{\omega} = \frac{1}{2\tau} S(\tau) \tag{56}$$

and

$$\tilde{\gamma} = \frac{1}{2\tau}[1 - C(\tau)], \tag{57}$$

with $C(t)$ and $S(t)$ defined in Eq. (25). In order for this approximation to be justified, it is required that the coarse-graining time scale τ be much larger than any characteristic time scale of the bath [32]. However, in our case the bath correlation time is infinite which, once again, shows the inapplicability of the Markovian approximation. This is further supported by the performance of the optimal solution that one can achieve by varying τ, which is discussed in Sec. IV. There we numerically examine the average trace-distance between the solution to Eq. (55) and the exact solution as a function of τ. The average is taken over a time T, which is greater than the decay time of the exact solution. We determine an optimal τ for which the average trace distance is minimum and then determine the approximate solution. The solution of Eq. (55) for a particular τ in terms of the Bloch vector components is

$$\begin{aligned} v_x(t) &= v_x(0)\tilde{C}_\tau(t) + v_y(0)\tilde{S}_\tau(t), \\ v_y(t) &= v_y(0)\tilde{C}_\tau(t) - v_x(0)\tilde{S}_\tau(t), \end{aligned} \tag{58}$$

where $\tilde{C}_\tau(t) = e^{-\tilde{\gamma}(\tau)t}\cos[\tilde{\omega}(\tau)t]$ and $\tilde{S}_\tau(t) = e^{-\tilde{\gamma}(\tau)t}\sin[\tilde{\omega}(\tau)t]$. The average trace distance as a function of τ is given by

$$\begin{aligned} \bar{D}(\rho_{\text{exact}}, \rho_{\text{CG}}) &\equiv \frac{1}{2}\text{Tr}|\rho_{\text{exact}} - \rho_{\text{CG}}| \\ &= \frac{1}{2T}\sum_{t=0}^{T} \sqrt{[C(t) - \tilde{C}(t)]^2 + [S(t) - \tilde{S}(t)]^2} \\ &\quad \times \sqrt{v_x(0)^2 + v_y(0)^2}, \end{aligned} \tag{59}$$

where ρ_{CG} represents the coarse-grained solution and where $|X| = \sqrt{X^\dagger X}$. The results are presented in Sec. IV. Next we consider the Nakajima-Zwanzig (NZ) and the time-convolutionless (TCL) master equations for higher-order approximations.

B. NZ and TCL master equations

Using projection operators one can obtain approximate non-Markovian master equations to higher orders in αt. A projection is defined as follows:

$$\mathcal{P}\rho = \text{Tr}_B\{\rho\} \otimes \rho_B, \tag{60}$$

and serves to focus on the "relevant dynamics" (of the system) by removing the bath (a recent generalization is discussed in Ref. [35]). The choice of ρ_B is somewhat arbitrary and can be taken to be $\rho_B(0)$, which significantly simplifies the calculations. Using the notation introduced in [16], define

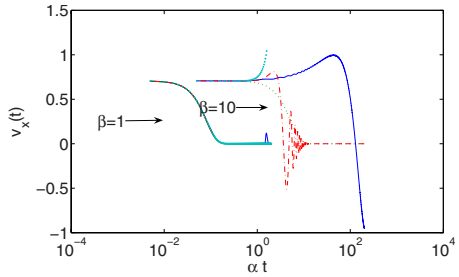

FIG. 7. (Color online) Comparison of the exact solution, TCL2, TCL3, and TCL4 at $\beta=1$ and $\beta=10$ for $N=100$. The exact solution is the solid (blue) line, TCL2 is the dashed (green) line, TCL3 is the dot-dashed (red) line, and TCL4 is the dotted (cyan) line. Note that for $\beta=1$, the curves nearly coincide.

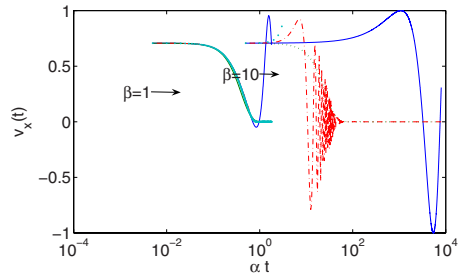

FIG. 8. (Color online) Comparison of the exact solution, TCL2, TCL3, and TCL4 at $\beta=1$ and $\beta=10$ for $N=4$. The exact solution is the solid (blue) line, TCL2 is the dashed (green) line, TCL3 is the dot-dashed (red) line, and TCL4 is the dotted (cyan) line. Note that for $\beta=1$, TCL3, TCL4, and the exact solution nearly coincide.

$$\mathcal{S} \equiv \mathcal{PSP} \tag{61}$$

for any superoperator $\mathcal{S}$. Thus $\langle \mathcal{S}^n \rangle$ denote the moments of the superoperator. Note that for the Liouvillian superoperator, $\langle \mathcal{L} \rangle = 0$ by virtue of the fact that $\mathrm{Tr}_B\{B\rho_B(0)\}=0$ (see [2]). Since we assume that the initial state is a product state, both the NZ and TCL equations are homogeneous equations. The NZ master equation is an integrodifferential equation with a memory kernel $\mathcal{N}(t,s)$ and is given by

$$\dot{\rho}_S(t) \otimes \rho_B = \int_0^t \mathcal{N}(t,s)\rho_S(s) \otimes \rho_B ds. \tag{62}$$

The TCL master equation is a time-local equation given by

$$\dot{\rho}_S(t) \otimes \rho_B = \mathcal{K}(t)\rho_S(t) \otimes \rho_B. \tag{63}$$

When these equations are expanded in αt and solved we obtain the higher-order corrections. When the interaction Hamiltonian is time independent (as in our case), the above equations simplify to

$$\int_0^t \mathcal{N}(t,s)\rho_S(s) \otimes \rho_B ds = \sum_{n=1}^{\infty} \alpha^n \mathcal{I}_n(t,s)\langle \mathcal{L}^n \rangle_{pc} \rho_S(s), \tag{64}$$

and

$$\mathcal{K}(t) = \sum_{n=1}^{\infty} \alpha^n \frac{t^{n-1}}{(n-1)!} \langle \mathcal{L}^n \rangle_{oc} \tag{65}$$

for the NZ and TCL equations, respectively, where the time-ordered integral operator $\mathcal{I}_n(t,s)$ is defined as

$$\mathcal{I}_n(t,s) \equiv \int_0^t dt_1 \int_0^{t_1} dt_2 \cdots \int_0^{t_{n-2}} ds. \tag{66}$$

The definitions of the partial cumulants $\langle \mathcal{L} \rangle_{pc}$ and the ordered cumulants $\langle \mathcal{L} \rangle_{oc}$ are given in Refs. [12,36,37]. For our model we have

$$\langle \mathcal{L} \rangle_{pc} = \langle \mathcal{L} \rangle_{oc} = 0, \tag{67}$$

and

$$\langle \mathcal{L}^2 \rangle_{pc} = \langle \mathcal{L}^2 \rangle,$$

$$\langle \mathcal{L}^2 \rangle_{oc} = \langle \mathcal{L}^2 \rangle,$$

$$\langle \mathcal{L}^3 \rangle_{pc} = \langle \mathcal{L}^3 \rangle,$$

$$\langle \mathcal{L}^3 \rangle_{oc} = \langle \mathcal{L}^3 \rangle,$$

$$\langle \mathcal{L}^4 \rangle_{pc} = \langle \mathcal{L}^4 \rangle - \langle \mathcal{L}^2 \rangle^2,$$

$$\langle \mathcal{L}^4 \rangle_{oc} = \langle \mathcal{L}^4 \rangle - 3\langle \mathcal{L}^2 \rangle^2. \tag{68}$$

Explicit expressions for these quantities are given in Appendix B. Substituting these into the NZ and TCL equations (64) and (65), we obtain what we refer to below as the NZn and TCLn master equations, with $n=2,3,4$. These approximate master equations are, respectively, second, third, and fourth order in the coupling constant α, and they can be solved analytically. The second-order solution of the NZ equation (NZ2) is exactly the Born approximation and the solution is given in Eq. (46). The third-order NZ master equation is given by

$$\dot{\rho}_S(t) = -2\alpha^2 Q_2 \mathcal{I}_2(t,s)[\rho_S(s) - \sigma^z \rho_S(s)\sigma^z] + i4\alpha^3 Q_3 \mathcal{I}_3(t,s) \times [\sigma^z \rho_S(s) - \rho_S(s)\sigma^z], \tag{69}$$

and the fourth order is

$$\dot{\rho}_S(t) = -2\alpha^2 Q_2 \mathcal{I}_2(t,s)[\rho_S(s) - \sigma^z \rho_S(s)\sigma^z] + i4\alpha^3 Q_3 \mathcal{I}_3(t,s) \times [\sigma^z \rho_S(s) - \rho_S(s)\sigma^z] + 8\alpha^4 (Q_4 - Q_2^2)\mathcal{I}_4(t,s)[\rho_S(s) - \sigma^z \rho_S(s)\sigma^z]. \tag{70}$$

These equations are equivalent to, respectively, sixth and eighth order differential equations (with constant coefficients) and are difficult to solve analytically. The results we present in the next section were therefore obtained numerically.

The situation is simpler in the TCL approach. The second-order TCL equation is given by

$$\dot{\rho}_S(t) = -\alpha^2 t\, \mathrm{Tr}_B\{[H_I,[H_I,\rho_S(t) \otimes \rho_B(0)]]\} = -2\alpha^2 t Q_2[\rho_S(t) - \sigma^z \rho_S(t)\sigma^z], \tag{71}$$

whose solution is as given in Eq. (48) in terms of Bloch vector components. For TCL3 we find

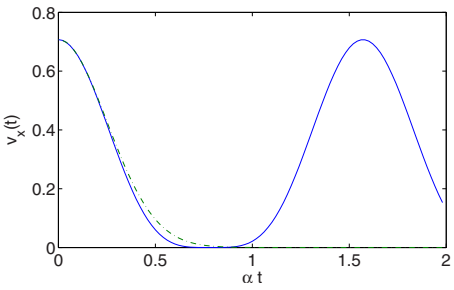

FIG. 9. (Color online) Comparison of TCL2 and the exact solution to demonstrate the validity of the TCL approximation for $N=4$ and $\beta=1$. The solid (blue) line denotes the exact solution and the dashed (green) line is TCL2. Note that the time axis here is on a linear scale. TCL2 breaks down at $\alpha t \approx 0.9$, where it remains flat, while the exact solution has a recurrence.

$$\dot{\rho}_S(t) = -2\alpha^2 t Q_2[\rho_S(t) - \sigma_z \rho_S(t)\sigma_z] + 4iQ_3\alpha^3\frac{t^2}{2}[\sigma_z\rho_S(t) - \rho_S(t)\sigma_z], \tag{72}$$

and for TCL4 we find

$$\dot{\rho}_S(t) = \left[-2\alpha^2 t Q_2 + (8Q_4 - 24Q_2^2)\alpha^4\frac{t^3}{6}\right] \times [\rho_S(t) - \sigma_z\rho_S(t)\sigma_z] + 4iQ_3\alpha^3\frac{t^2}{2} \times [\sigma_z\rho_S(t) - \rho_S(t)\sigma_z]. \tag{73}$$

These equation can be solved analytically, and the solutions to the third- and fourth-order TCL equations are given by

$$v_x(t) = f_n(\alpha t)[v_x(0)\cos(g(t)) + v_y(0)\sin(g(t))],$$
$$v_y(t) = f_n(\alpha t)[v_y(0)\cos(g(t)) - v_x(0)\sin(g(t))], \tag{74}$$

where $g(t)=4Q_3\alpha^3 t^3/3$, $f_3(\alpha t)=\exp(-2Q_2\alpha^2 t^2)$ (TCL3), and $f_4(\alpha t)=\exp[-2Q_2\alpha^2 t^2+(2Q_4-6Q_2^2)\alpha^4 t^4/3]$ (TCL4). It is interesting to note that the second-order expansions of the TCL and NZ master equations exhibit a $v_x \leftrightarrow v_y$ symmetry between the components of the Bloch vector, and only the third-order correction breaks this symmetry. Notice that the coefficient of α^3 does not vanish in this model unlike in the one considered in [16] because both $\langle \mathcal{L}^3\rangle_{pc} \neq 0$ and $\langle \mathcal{L}^3\rangle_{oc} \neq 0$ and hence the third-order (and other odd order) approximations exist.

C. Post-Markovian (PM) master equation

In this section we study the performance of the post-Markovian master equation recently proposed in [13].

$$\frac{\partial\rho(t)}{\partial t} = \mathcal{D}\int_0^t dt' k(t')\exp(\mathcal{D}t')\rho(t-t'). \tag{75}$$

This equation was constructed via an interpolation between the exact dynamics and the dynamics in the Markovian limit. The operator $\mathcal{D}$ is the dissipator in the Lindblad equation (50), and $k(t)$ is a phenomenological memory kernel, which must be found by fitting to data or guessed on physical grounds. As was discussed earlier, the Markovian approximation fails for our model, nevertheless, one can use the form of the dissipator we obtained in Eq. (50),

$$\mathcal{D}\rho = \sigma^z\rho\sigma^z - \rho. \tag{76}$$

It is interesting to examine to what extent Eq. (75) can approximate the exact dynamics. As a measure of the performance of the post-Markovian equation, we will take the trace distance between the exact solution $\rho_{\text{exact}}(t)$ and the solution to the post-Markovian equation $\rho_1(t)$. The general solution of Eq. (75) can be found by expressing $\rho(t)$ in the damping basis [38] and applying a Laplace transform [13]. The solution is

$$\rho(t) = \sum_i \mu_i(t)R_i = \sum_i \mathrm{Tr}(L_i\rho(t))R_i, \tag{77}$$

where

$$\mu_i(t) = \mathrm{Lap}^{-1}\left[\frac{1}{s-\lambda_i\tilde{k}(s-\lambda_i)}\right]\mu_i(0) \equiv \xi_i(t)\mu_i(0), \tag{78}$$

(Lap^{-1} is the inverse Laplace transform) with $\tilde{k}$ being the Laplace transform of the kernel k, $\{L_i\}$ and $\{R_i\}$ being the left and right eigenvectors of the superoperator $\mathcal{D}$, and λ_i the corresponding eigenvalues. For our dissipator the damping basis is $\{L_i\}=\{R_i\}=\left\{\frac{I}{\sqrt{2}},\frac{\sigma^x}{\sqrt{2}},\frac{\sigma^y}{\sqrt{2}},\frac{\sigma^z}{\sqrt{2}}\right\}$ and the eigenvalues are $\{0,-2,-2,0\}$. Therefore, we can immediately write the formal solution in terms of the Bloch vector components as follows:

$$v_{x,y}(t) = \mathrm{Lap}^{-1}\left[\frac{1}{s+2\tilde{k}(s+2)}\right]v_{x,y}(0) \equiv \xi(t)v_{x,y}(0). \tag{79}$$

We see that $v_x(t)$ has no dependence on $v_y(0)$, and neither does $v_y(t)$ on $v_x(0)$, in contrast to the exact solution. The difference comes from the fact that the dissipator $\mathcal{D}$ does not couple $v_x(t)$ and $v_y(t)$. This reveals an inherent limitation of the post-Markovian master equation: it inherits the symmetries of the Markovian dissipator $\mathcal{D}$, which may differ from those of the generator of the exact dynamics. In order to rigorously determine the optimal performance, we use the trace distance between the exact solution and a solution to the post-Markovian equation as follows:

$$D(\rho_{\text{exact}}(t),\rho_1(t)) = \frac{1}{2}\sqrt{[C(t)-\xi(t)]^2 + S(t)^2} \times \sqrt{v_x(0)^2 + v_y(0)^2}. \tag{80}$$

Obviously this quantity reaches its minimum for $\xi(t)=C(t)$, $\forall t$ independently of the initial conditions. The kernel for which the optimal performance of the post-Markovian master equation is achieved, can thus be formally expressed, using Eq. (79), as

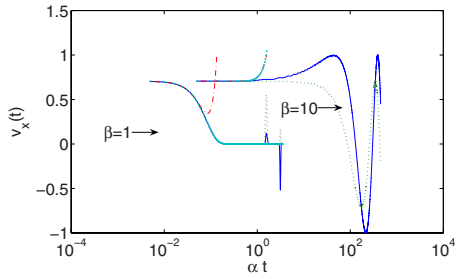

FIG. 10. (Color online) Comparison of the exact solution, NZ4, TCL4, and PM at $\beta=1$ and $\beta=10$ for $N=100$. The exact solution is the solid (blue) line, PM is the dashed (green) line, NZ4 is the dot-dashed (red) line, and TCL4 is the dotted (cyan) line. Note that for $\beta=1$, TCL4, PM, and the exact solution nearly coincide for short and medium times. Only PM captures the recurrences of the exact solution at long times.

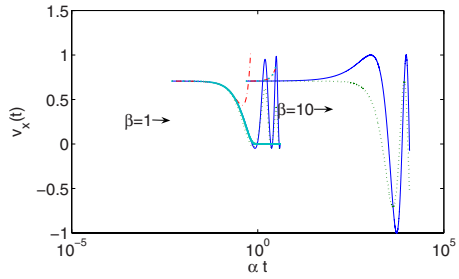

FIG. 11. (Color online) Comparison of the exact solution, NZ4, TCL4, and PM at $\beta=1$ and $\beta=10$ for $N=4$. The exact solution is the solid (blue) line, PM is the dashed (green) line, NZ4 is the dot-dashed (red) line, and TCL4 is the dotted (cyan) line. Note that for $\beta=1$, TCL4 and the exact solution nearly coincide for short and medium times.

$$k_{\mathrm{opt}}(t) = \frac{1}{2}e^{2t}\,\mathrm{Lap}^{-1}\left\{\frac{1}{\mathrm{Lap}(C(t))} - s\right\}. \tag{81}$$

It should be noted that the condition for complete positivity of the map generated by Eq. (75), $\Sigma_i \xi_i(t) L_i^T \otimes R_i \geqslant 0$ [13], amounts here to $|\xi(t)| = |C(t)| \leqslant 1$, which holds for all t. Thus the minimum achievable trace distance between the two solutions is given by

$$D_{\min}(\rho_{\mathrm{exact}}(t), \rho_1(t)) = \frac{1}{2}S(t)\sqrt{v_x(0)^2 + v_y(0)^2}. \tag{82}$$

The optimal fit is plotted in Sec. IV.

Finding a simple analytical expression for the optimal kernel Eq. (81) seems difficult due to the complicated form of $C(t)$. One way to approach this problem is to expand $C(t)$ in powers of αt and consider terms which give a valid approximation for small times $\alpha t \ll 1$. For example, Eq. (33) yields the lowest nontrivial order as

$$C_2(t) = 1 - 2Q_2\alpha^2 t^2 + O(\alpha^4 t^4). \tag{83}$$

Note that this solution violates the complete positivity condition for times larger than $t = 1/\alpha\sqrt{2Q_2}$. The corresponding kernel is

$$k_2(t) = 2\alpha^2 Q_2 e^{2t}\cosh(2\sqrt{Q_2}\alpha t). \tag{84}$$

Alternatively we could try finding a kernel that matches some of the approximate solutions discussed so far. For example, it turns out that the kernel

$$k_{\mathrm{NZ2}}(t) = 2\alpha^2 Q_2 e^{2t} \tag{85}$$

leads to an exact match of the NZ2 solution. Finding a kernel which gives a good description of the evolution of an open system is an important but in general, difficult question which remains open for further investigation. We note that this question was also taken up in the context of the PM in the recent study [39], where the PM was applied to an exactly solvable model describing a qubit undergoing spontaneous emission and stimulated absorption. No attempt was made to optimize the memory kernel and hence the agreement with the exact solution was not as impressive as might be possible with optimization.

Finally, we stress again that $k(t)$ is a phenomenological memory kernel which must be found either by fitting or by guessing. As pointed out in Ref. [13], experimental determination of the kernel by fitting can be done as follows. Suppose one measures $\rho(t)$ via quantum state tomography. It can be shown that $\xi_i(t) = \mathrm{Tr}[L_i\rho(t)]/\mathrm{Tr}[L_i\rho(0)]$ [13]. The coefficients $\xi_i(t)$ are thus directly experimentally accessible, provided one first specifies a Markovian model from which the left eigenvectors L_i and eigenvalues λ_i can be computed. Inverting Eq. (78) then yields the kernel as

$$k(t) = \mathrm{Lap}^{-1}[(s - 1/\mathrm{Lap}[\xi_i(t)])]e^{-\lambda_i t}/\lambda_i.$$

This inversion process for $k(t)$ is not unique in the sense that it will depend on the choice of Markovian model. It can be optimized via well-established maximum likelihood methods, e.g., [40], thus yielding the optimal Markovian model. Another possibility for determining $k(t)$ in a systematic fashion is to attempt to find a general analytical optimal fit between the PM master equation and the TCL or NZ master equations.

IV. COMPARISON OF THE ANALYTICAL SOLUTION AND THE DIFFERENT APPROXIMATION TECHNIQUES

In the results shown below, all figures express the evolution in terms of the dimensionless parameter αt (plotted on a logarithmic scale). We choose the initial condition $v_x(0) = v_y(0) = 1/\sqrt{2}$ and plot only $v_x(t)$ since the structure of the equations for $v_x(t)$ and $v_y(t)$ is similar. In order to compare the different methods of approximation, we consider various choices of parameter values in our model. Among these choices we consider both low- and high-temperature cases. We note that in a spin-bath model it is assumed that the environment degrees of freedom are localized and this is usually the case at low temperatures. At higher temperatures one may need to consider delocalized environment degrees of freedom as well, such as phonons, magnons, etc. A class of models known as oscillator bath models [41] incorporate such effects. In this paper, we restrict attention to the spin-

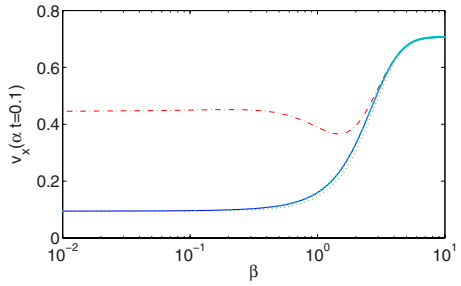

FIG. 12. (Color online) Comparison of the exact solution, NZ4, TCL4, and PM at $\alpha t=0.1$ for $N=100$ for different $\beta \in [0.01, 10]$. The exact solution is the solid (blue) line, PM is the dashed (green) line, NZ4 is the dot-dashed (red) line, and TCL4 is the dotted (cyan) line.

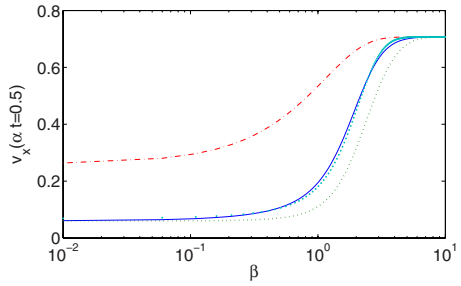

FIG. 13. (Color online) Comparison of the exact solution, NZ4, TCL4, and PM at $\alpha t=0.5$ for $N=4$ for different $\beta \in [0.01, 10]$. The exact solution is the solid (blue) line, PM is the dashed (green) line, NZ4 is the dot-dashed (red) line, and TCL4 is the dotted (cyan) line.

bath model described here for both low and high temperatures, as our primary goal is not a realistic description of decoherence in solid state systems, but a comparison of different master equations to an exactly solvable model.

A. Exact solution

We first assume that the frequencies of the qubits in the bath are equal ($\Omega_n=1$, $\forall$ n), and so are the coupling constants ($g_n=1$, $\forall$ n). In this regime, we consider large and small numbers of bath spins $N=100$ and $N=4$, and two different temperatures $\beta=1$ and $\beta=10$. Figures 1 and 2 show the exact solution for $N=100$ and $N=4$ spins, respectively, up to the second recurrence time. For each N, we plot the exact solution for $\beta=1$ and $\beta=10$.

We also consider the case where the frequencies Ω_n and the coupling constants g_n can take different values. We generated uniformly distributed random values in the interval $[-1,1]$ for both Ω_n and g_n. In Figures 3 and 4 we plot the ensemble average of the solution over 50 random ensembles. The main difference from the solution with equal Ω_n and g_n is that the partial recurrences decrease in size, especially as N increases. We attribute this damping partially to the fact that we look at the ensemble average, which amounts to averaging out the positive and negative oscillations that arise for different values of the parameters. The main reason, however, is that for a generic ensemble of random Ω_n and g_n the positive and negative oscillations in the sums (25) tend to average out. This is particularly true for large N, as reflected in Fig. 3. We looked at a few individual random cases for $N=100$ and recurrences were not present there. For $N=20$ (not shown here), some small recurrences were still visible.

We also looked at the case where one of the coupling constants, say g_i, has a much larger magnitude than the other ones (which were made equal). The behavior was similar to that for a bath consisting of only a single spin.

In the following, we plot the solutions of different orders of the NZ, TCL, and PM master equations and compare them for the same parameter values.

B. NZ

In this section, we compare the solutions of different orders of the NZ master equation for $\Omega_n=g_n=1$. Figure 5 shows the solutions to NZ2, NZ3, NZ4 and the exact solution for $\beta=1$ and $\beta=10$ up to the first recurrence time of the exact solution. For short times NZ4 is the better approximation. It can be seen that while NZ2 and NZ3 are bounded, NZ4 leaves the Bloch sphere. But note that the approximations under which these solutions have been obtained are valid for $\alpha t \ll 1$. The NZ4 solution leaves the Bloch sphere in a regime where the approximation is not valid. For $\beta=10$, NZ2 again has a periodic behavior (which is consistent with the solution), while the NZ3 and NZ4 solutions leave the Bloch sphere after small times. Figure 6 shows the same graphs for $N=4$. In this case both NZ3 and NZ4 leave the Bloch sphere for $\beta=1$ and $\beta=10$, while NZ2 has a periodic behavior. A clear conclusion from these plots is that the NZ approximation is truly a short-time one: it becomes completely unreliable for times longer than $\alpha t \ll 1$.

C. TCL

Figure 7 plots the exact solution, TCL2, TCL3, and TCL4 at $\beta=1$ and $\beta=10$ for $N=100$ spins and $\Omega_n=g_n=1$. It can be seen that for $\beta=1$, the TCL solution approximates the exact solution well even for long times. However, the TCL solution cannot reproduce the recurrence behavior of the exact solution (also shown in the figure.) Figure 8 shows the same graphs for $N=4$. In this case, while TCL2 and TCL3 decay, TCL4 increases exponentially and leaves the Bloch sphere after a short time. This is because the exponent in the solution of TCL4 in Eq. (74) is positive. Here again the approximations under which the solutions have been obtained are valid only for small time scales and the graphs demonstrate the complete breakdown of the perturbation expansion for large values of αt. Moreover, the graphs reveal the sensitivity of the approximation to temperature: the TCL fares much better at high temperatures.

In order to determine the validity of the TCL approximation, we look at the invertibility of the Kraus map derived in Eq. (18) or equivalently Eq. (25). As mentioned earlier, this map is noninvertible if $C(t)^2+S(t)^2=0$ for some t [or equivalently $v_x(t)=0$ and $v_y(t)=0$]. This will happen if and only if at least one of the β_n is zero. This can occur when the bath density matrices of some of the bath spins are maximally mixed or in the limit of a very high bath temperature. Clearly, when the Kraus map is noninvertible, the TCL ap-

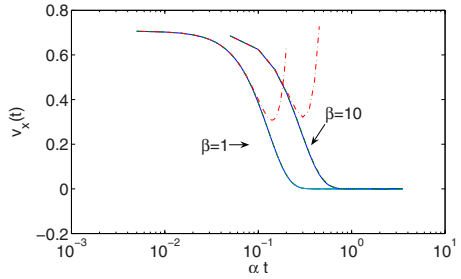

FIG. 14. (Color online) Comparison of the exact solution, NZ4, TCL4, and PM at $\beta=1$ and $\beta=10$ for $N=100$ for random values of g_n and Ω_n. The exact solution is the solid (blue) line, PM is the dashed (green) line, NZ4 is the dot-dashed (red) line, and TCL4 is the dotted (cyan) line. Note that for $\beta=1$ and $\beta=10$, TCL4, PM, and the exact solution nearly coincide.

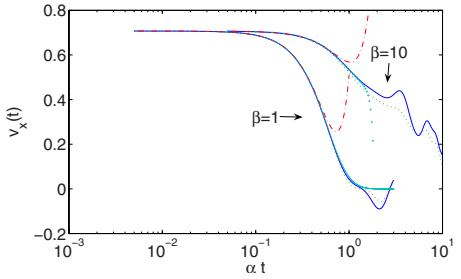

FIG. 15. (Color online) Comparison of the exact solution, NZ4, TCL4, and PM at $\beta=1$ and $\beta=10$ for $N=4$ for random values of g_n and Ω_n. The exact solution is the solid (blue) line, PM is the dashed (green) line, NZ4 is the dot-dashed (red) line, and TCL4 is the dotted (cyan) line. Note that for $\beta=1$, TCL4, PM, and the exact solution nearly coincide for short and medium times.

proach becomes invalid since it relies on the assumption that the information about the initial state is contained in the current state. This fact has also been observed for the spin-boson model with a damped Jaynes-Cummings Hamiltonian [2]. At the point where the Kraus map becomes noninvertible, the TCL solution deviates from the exact solution (see Fig. 9). We verified that both v_x and v_y vanish at this point.

D. NZ, TCL, and PM

In this section, we compare the exact solution to TCL4, NZ4, and the solution of the optimal PM master equation. Figure 10 shows these solutions for $N=100$ and $\beta=1$ and $\beta=10$ when $\Omega_n=g_n=1$. Here we observe that while the short-time behavior of the exact solution is approximated well by all the approximations we consider, the long-time behavior is approximated well only by PM.

For $\beta=1$, NZ4 leaves the Bloch sphere after a short time while TCL4 decays with the exact solution. But as before, the TCL solution cannot reproduce the recurrences seen in the exact solution. The optimal PM solution, by contrast, is capable of reproducing both the decay and the recurrences. TCL4 and NZ4 leave the Bloch sphere after a short time for $\beta=10$, while PM again reproduces the recurrences in the exact solution. Figure 11 shows the corresponding graphs for $N=4$ and it can be seen that again PM can outperform both TCL and NZ for long times. Figures 12 and 13 show the performance of TCL4, NZ4, and PM compared to the exact solution at a fixed time (for which the approximations are valid) for different temperatures ($\beta \in [0.01, 10]$). It can be seen that both TCL4 and the optimal PM solution perform better than NZ4 at medium and high temperatures, with TCL4 outperforming PM at medium temperatures. The performance of NZ4 is enhanced at low temperatures, where it performs similarly to TCL4 (see also Figs. 10 and 11). This can be understood from the short-time approximation to the exact solution given in Eq. (37), which up to the precision for which it was derived is also an approximation of NZ2 [Eq. (46)]. As discussed above, this approximation (which also coincides with TCL2) is valid when $2Q_2(\alpha t)^2 \ll 1$. As temperature decreases, so does the magnitude of Q_2, which leads to a better approximation at fixed αt. Since NZ2 gives the lowest-order correction, this improvement is reflected in NZ4 as well.

In Figs. 14 and 15 we plot the averaged solutions over 50 ensembles of random values for Ω_n and g_n in the interval $[-1,1]$. We see that on average TCL4, NZ4, and the optimal PM solution behave similarly to the case when $\Omega_n=g_n=1$. Due to the damping of the recurrences, especially when $N=100$, the TCL4 and the PM solutions match the exact solution closely for much longer times than in the deterministic case. Again, the PM solution is capable of qualitatively matching the behavior of the exact solution at long times.

E. Coarse-graining approximation

Finally, we examine the coarse-graining approximation discussed in Sec. III. We choose the time over which the average trace distance is calculated to be the time where the exact solution dies down. In Fig. 16 we plot the coarse-grained solution for the value of τ for which the trace distance to the exact solution is minimum. As can be seen, the coarse-graining approximation does not help since the Markovian assumption is not valid for this model. In deriving the coarse-graining approximation [32] one makes the assumption that the coarse-graining time scale is greater than any characteristic bath time scale. But the characteristic time scale of the bath is infinite in this case.

V. SUMMARY AND CONCLUSIONS

We studied the performance of various methods for approximating the evolution of an Ising model of an open quantum system for a qubit system coupled to a bath consisting of N qubits. The high symmetry of the model allowed us to derive the exact dynamics of the system as well as find analytical solutions for the different master equations. We saw that the Markovian approximation fails for this model due to the time independence of the bath correlation functions. This is also reflected in the fact that the coarse-graining method [32] does not approximate the exact solution well. We discussed the performance of these solutions for various parameter regimes. Unlike other spin-bath models discussed in literature (e.g., [16]), the odd-order bath cor-

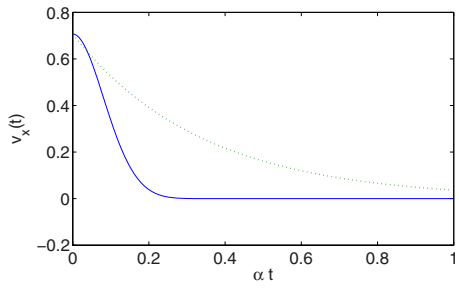

FIG. 16. (Color online) Comparison of the exact solution and the optimal coarse-graining approximation for $N=50$ and $\beta=1$. The exact solution is the solid (blue) line and the coarse-graining approximation is the dashed (green) line. Note the linear scale time axis.

relation functions do not vanish, leading to the existence of odd-order terms in the solution of TCL and NZ equations. These terms describe the rotation around the z axis of the Bloch sphere, a fact which is reflected in the exact solution. We showed that up to fourth order TCL performs better than NZ at medium and high temperatures. For low temperatures we demonstrated an enhancement in the performance of NZ and showed that NZ and TCL perform equally well. We showed that the TCL approach breaks down for certain parameter choices and related this to the noninvertibility of the Kraus map describing the system dynamics. We also studied the performance of the post-Markovian master equation obtained in [13] with an optimal memory kernel. We discussed possible ways of approximating the optimal kernel for short times and derived the kernel which leads to an exact fit to the NZ2 solution. It turns out that PM master equation performs as well as the TCL2 for a large number of spins and outperforms all orders of NZ and TCL considered here at long times, as it captures the recurrences of the exact solution.

Our study reveals the limitations of some of the best known master equations available in the literature, in the context of a spin bath. In general, perturbative approaches such as low-order NZ and TCL do well at short times (on a time scale set by the system-bath coupling constant) and fare very poorly at long times. These approximations are also very sensitive to temperature and do better in the high-temperature limit. The PM does not do as well as TCL4 at short times but has the distinct advantage of retaining a qualitatively correct character for long times. This conclusion depends heavily on the proper choice of the memory kernel; indeed, when the memory kernel is not optimally chosen the PM can yield solutions which are not as satisfactory [39].

ACKNOWLEDGMENTS

O.O. and H.K. were supported in part by NSF Grant No. CCF-0524822, and H.K. was also supported in part by NSF Grant No. CCF-0448658. D.A.L. was supported by NSF Grant No. CCF-0523675 and CCF-0726439.

APPENDIX A: BATH CORRELATION FUNCTIONS

Here we show how to calculate the bath correlation functions used in our simulations. The kth-order bath correlation function is defined as

$$Q_k = \mathrm{Tr}\{B^k \rho_B\},$$

where B and ρ_B were given in Eqs. (16) and (12), respectively. This yields

$$\begin{aligned}
Q_k &= \mathrm{Tr}\left\{\left(\sum_n g_n\sigma_n^z - \theta I_B\right)^k \sum_l \frac{\exp(-\beta E_l)}{Z}|l\rangle\langle l|\right\} \\
&= \sum_l \frac{\exp(-\beta E_l)}{Z}\langle l|\left(\sum_n g_n\sigma_n^z - \theta I_B\right)^k|l\rangle \\
&= \sum_{l,l',\ldots,l'''} \frac{\exp(-\beta E_l)}{Z}\langle l|\left(\sum_n g_n\sigma_n^z - \theta I_B\right)|l'\rangle\langle l'|\left(\sum_{n'} g_{n'}\sigma_{n'}^z - \theta I_B\right)|l''\rangle\langle l''|\cdots|l'''\rangle\langle l'''|\left(\sum_{n'''} g_{n'''}\sigma_{n'''}^z - \theta I_B\right)|l\rangle \\
&= \sum_{l,l',\ldots,l'''} \frac{\exp(-\beta E_l)}{Z}\left(\sum_n g_n\langle l|\sigma_n^z|l'\rangle - \theta\right)\delta_{ll'}\left(\sum_{n'} g_{n'}\langle l'|\sigma_{n'}^z|l''\rangle - \theta\right)\delta_{l'l''}\cdots\left(\sum_{n'''} g_{n'''}\langle l'''|\sigma_{n'''}^z|l\rangle - \theta\right)\delta_{l'''l} \\
&= \sum_l \frac{\exp(-\beta E_l)}{Z}\left(\sum_n g_n\langle l|\sigma_n^z|l\rangle - \theta\right)\left(\sum_{n'} g_{n'}\langle l|\sigma_{n'}^z|l\rangle - \theta\right)\cdots\left(\sum_{n'''} g_{n'''}\langle l|\sigma_{n'''}^z|l\rangle - \theta\right) \\
&= \sum_l \frac{\exp(-\beta E_l)}{Z}\left(\sum_n g_n\langle l|\sigma_n^z|l\rangle - \theta\right)^k,
\end{aligned}$$

or

$$Q_k = \frac{1}{Z}\sum_l (\tilde{E}_l)^k \exp(-\beta E_l), \tag{A1}$$

where $Z=\Sigma_l \exp(-\beta E_l)$ and the expressions for E_l and $\tilde{E}_l$ were given in Eqs. (21) and (23), respectively.

The above formulas are useful when the energy levels E_l and $\tilde{E}_l$ are highly degenerate, which is the case, for example, when $g_n \equiv g$ and $\Omega_n \equiv \Omega$ for all n. For a general choice of these parameters, it is computationally more efficient to consider θ in the form (28) and the initial bath density matrix in the form (26). For example, the second-order bath correlation function is

$$\begin{aligned}
Q_2 &= \mathrm{Tr}\left\{\left(\sum_{m=1}^{N} g_m\sigma_m^z - \theta I\right)\left(\sum_{n=1}^{N} g_n\sigma_n^z - \theta I\right)\rho_B\right\} \\
&= \mathrm{Tr}\left\{\sum_{n,m=1}^{N} g_n g_m \sigma_n^z\sigma_m^z\rho_B\right\} - 2\theta\underbrace{\mathrm{Tr}\left\{\sum_{n=1}^{N} g_n\sigma_n^z\rho_B\right\}}_{\theta} + \theta^2 \\
&= \mathrm{Tr}\left\{\sum_{n,m=1}^{N} g_n g_m \sigma_n^z\sigma_m^z \bigotimes_{n=1}^{N}\frac{1}{2}(I+\beta_n\sigma_n^z)\right\} - \theta^2 \\
&= \sum_{n\neq m}^{N}\mathrm{Tr}\left\{g_m\frac{1}{2}(\sigma_m^z+\beta_m I)\right\}\mathrm{Tr}\left\{g_n\frac{1}{2}(\sigma_n^z+\beta_n I)\right\} \\
&\quad\times\prod_{j\neq m,n}\mathrm{Tr}\left\{\frac{1}{2}(I+\beta_j\sigma_j^z)\right\} + \mathrm{Tr}\left\{\sum_{n=1}^{N} g_n^2\rho_B\right\} - \theta^2 \\
&= \underbrace{\sum_{n,m=1}^{N} g_m\beta_m g_n\beta_n}_{\theta^2} - \sum_{n=1}^{N} g_n^2\beta_n^2 + \sum_{n=1}^{N} g_n^2 - \theta^2 = \sum_{n=1}^{N} g_n^2(1-\beta_n^2).
\end{aligned} \tag{A2}$$

Using the identity $1-\tanh^2(-x/2)=2/(1+\cosh x)$, this correlation function can be expressed in terms of the bath spectral density function [Eq. (13)] as follows:

$$\begin{aligned}
Q_2 &= \sum_{n=1}^{N} g_n^2(1-\beta_n^2) \\
&= \int_{-\infty}^{\infty}\delta(\Omega-\Omega_n)|g_n|^2 \\
&\quad\times\left[1-\tanh^2\left(-\frac{\Omega}{2kT}\right)\right]d\Omega \\
&= \int_{-\infty}^{\infty}\frac{2J(\Omega)d\Omega}{1+\cosh\left(\frac{\Omega}{kT}\right)}.
\end{aligned}$$

Higher-order correlation functions are computed analogously.

APPENDIX B: CUMULANTS FOR THE NZ AND TCL MASTER EQUATIONS

We calculate the explicit expressions for the cumulants appearing in Eq. (68), needed to find the NZ and TCL perturbation expansions up to fourth order.

Second order,

$$\begin{aligned}
\langle\mathcal{L}^2\rangle\rho &= -\mathrm{Tr}_B\{[H_I,[H_I,\rho]]\}\otimes\rho_B \\
&= -\mathrm{Tr}_B\{H_I^2\rho - 2H_I\rho H_I + \rho H_I^2\}\otimes\rho_B \\
&= -2Q_2(\rho_S - \sigma_z\rho_S\sigma_z)\otimes\rho_B \\
&\equiv \rho',
\end{aligned}$$

$$\begin{aligned}
\langle\mathcal{L}^2\rangle^2\rho &= \mathcal{P}\mathcal{L}^2\mathcal{P}\mathcal{P}\mathcal{L}^2\mathcal{P}\rho = \mathcal{P}\mathcal{L}^2\mathcal{P}\rho' \\
&= -2Q_2(\rho_S' - \sigma_z\rho_S'\sigma_z)\otimes\rho_B,
\end{aligned} \tag{B1}$$

where $\rho_S' = \mathrm{Tr}_B\rho' = -2Q_2(\rho_S - \sigma_z\rho_S\sigma_z)$. Therefore

$$\begin{aligned}
\langle\mathcal{L}^2\rangle^2\rho &= -2Q_2\{[-2Q_2(\rho_S \\
&\quad - \sigma_z\rho_S\sigma_z)] - \sigma_z[-2Q_2(\rho_S \\
&\quad - \sigma_z\rho_S\sigma_z)]\sigma_z\}\otimes\rho_B \\
&= 8Q_2^2(\rho_S - \sigma_z\rho_S\sigma_z)\otimes\rho_B.
\end{aligned} \tag{B2}$$

Third order,

$$\begin{aligned}
\langle\mathcal{L}^3\rangle\rho &= i\mathrm{Tr}_B\{[H_I,[H_I,[H_I,\rho]]]\}\otimes\rho_B = i\mathrm{Tr}_B\{H_I^3\rho - 3H_I^2\rho H_I \\
&\quad + 3H_I\rho H_I^2 - \rho H_I^3\}\otimes\rho_B = 4iQ_3(\sigma_z\rho_S - \rho_S\sigma_z)\otimes\rho_B.
\end{aligned} \tag{B3}$$

Fourth order,

$$\begin{aligned}
\langle\mathcal{L}^4\rangle\rho &= \mathrm{Tr}_B\{[H_I,[H_I,[H_I,[H_I,\rho]]]]\}\otimes\rho_B = \mathrm{Tr}_B\{H_I^4\rho \\
&\quad - 4H_I^3\rho H_I + 6H_I^2\rho H_I^2 - 4H_I\rho H_I^3 + \rho H_I^4\}\otimes\rho_B \\
&= 8Q_4(\rho_S - \sigma_z\rho_S\sigma_z)\otimes\rho_B.
\end{aligned} \tag{B4}$$

[1] R. Alicki and K. Lendi, *Quantum Dynamical Semigroups and Applications*, Lecture Notes in Physics Vol. 286 (Springer-Verlag, Berlin, 1987).

[2] H.-P. Breuer and F. Petruccione, *The Theory of Open Quantum Systems* (Oxford University Press, Oxford, 2002).

[3] N. V. Prokof'ev and P. C. E. Stamp, Rep. Prog. Phys. **63**, 669 (2000).

[4] B. E. Kane, Nature (London) **393**, 133 (1998).

[5] R. Vrijen, E. Yablonovitch, K. Wang, H. W. Jiang, A. Balandin, V. Roychowdhury, T. Mor, and D. DiVincenzo, Phys. Rev. A **62**, 012306 (2000).

[6] D. Loss and D. P. DiVincenzo, Phys. Rev. A **57**, 120 (1998).

[7] R. de Sousa and S. Das Sarma, Phys. Rev. B **68**, 115322 (2003).

[8] W. M. Witzel and S. Das Sarma, Phys. Rev. B **74**, 035322 (2006).

[9] S. Nakajima, Prog. Theor. Phys. **20**, 948 (1958).

[10] R. Zwanzig, J. Chem. Phys. **33**, 1338 (1960).

[11] F. Shibata, Y. Takahashi, and N. Hashitsume, J. Stat. Phys. **17**, 171 (1977).
[12] F. Shibata and T. Arimitsu, J. Phys. Soc. Jpn. **49**, 891 (1980).
[13] A. Shabani and D. A. Lidar, Phys. Rev. A **71**, 020101(R) (2005).
[14] H. J. Carmichael, *Statistical Methods in Quantum Optics 1: Master Equations and Fokker-Planck Equations* (Springer, Berlin, 1999).
[15] C. Slichter, *Principles of Magnetic Resonance*, Springer Series in Solid-State Sciences Vol. 1 (Springer, Berlin, 1996).
[16] H.-P. Breuer, D. Burgarth, and F. Petruccione, Phys. Rev. B **70**, 045323 (2004).
[17] A. A. Budini and H. Shomerus, J. Phys. A **38**, 9251 (2005).
[18] A. A. Budini, J. Phys. B **40**, 2671 (2007).
[19] R. Alicki, M. Horodecki, P. Horodecki, and R. Horodecki, Phys. Rev. A **65**, 062101 (2002).
[20] F. J. Rodriguez, L. Quiroga, and N. F. Johnson, Phys. Rev. B **66**, 161302(R) (2002).
[21] F. J. Rodriguez, L. Quiroga, and N. F. Johnson, Europhys. Lett. **77**, 50009 (2007).
[22] R. Alicki, Phys. Rev. A **40**, 4077 (1989).
[23] R. Alicki, M. Horodecki, P. Horodecki, R. Horodecki, L. Jacak, and P. Machnikowski, Phys. Rev. A **70**, 010501(R) (2004).
[24] K. Shiokawa and B. L. Hu, Phys. Rev. A **70**, 062106 (2004).
[25] S. Shresta, C. Anastopoulos, A. Dragulescu, and B. L. Hu, Phys. Rev. A **71**, 022109 (2005).
[26] F. Palumbo *et al.*, Open Syst. Inf. Dyn. **13**, 309 (2006).
[27] D. Burgarth and S. Bose, Phys. Rev. A **73**, 062321 (2006).
[28] Y. Hamdouni, M. Fannes, and F. Petruccione, Phys. Rev. B **73**, 245323 (2006).
[29] X.-Z. Yuan, H. S. Goan, and K. D. Zhu, Phys. Rev. B **75**, 045331 (2007).
[30] S. Camalet and R. Chitra, Phys. Rev. B **75**, 094434 (2007).
[31] J. Jing and Z. G. Lu, Phys. Rev. B **75**, 174425 (2007).
[32] D. A. Lidar, Z. Bihary, and K. B. Whaley, Chem. Phys. **268**, 35 (2001).
[33] K. Kraus, *States, Effects and Operations, Fundamental Notions of Quantum Theory* (Academic, Berlin, 1983).
[34] H. Nakazato, M. Namiki, and S. Pascazio, Int. J. Mod. Phys. B **10**, 247 (1996).
[35] H.-P. Breuer, Phys. Rev. A **75**, 022103 (2007).
[36] A. Royer, Phys. Rev. A **6**, 1741 (1972).
[37] N. G. v. Kampen, Physica (Amsterdam) **74**, 239 (1974).
[38] H.-J. Briegel and B.-G. Englert, Phys. Rev. A **47**, 3311 (1993).
[39] S. Maniscalco and F. Petruccione, Phys. Rev. A **73**, 012111 (2006).
[40] K. Banaszek, G. M. D'Ariano, M. G. A. Paris, and M. F. Sacchi, Phys. Rev. A **61**, 010304(R) (1999).
[41] U. Weiss, *Quantum Dissipative Systems* (World Scientific, Singapore, 1999).